RSC Advances

PAPER

View Article Online
View Journal | View Issue



Cite this: *RSC Adv.*, 2025, **15**, 32546

# A dual-signal-amplified electrochemical biosensor for sensitive and accurate detection of cancer cells†

Yujuan Wu, [a] Yi Wang,[a] Rongxiang He,[c] Yu Li*[b] and Yali Ben*[a]

The accurate and highly sensitive detection of circulating tumor cells (CTCs) is crucial for cancer diagnosis, treatment, and metastasis monitoring. In this study, a dual-signal-amplified electrochemical biosensor specifically for identifying targeted CTCs. 3D polyvinylidene difluoride mixed with chitosan (PVDF/CS) nanofibers mesh was fabricated on polydimethylsiloxane (PDMS) micropillars using electrospinning technology. The nanofibers are modified with a graphene oxide-streptavidin-*anti*-epithelial adhesion molecule (GO-SA-EpCAM) antibody complex, which serves as an affinity molecule to capture the EpCAM positive cancer cells. Subsequently, a carboxylated multi-walled carbon nanotube-horseradish peroxidase-carbohydrate antigen 153 (MWCNTs-COOH-HRP-CA153) antibody complex is incubated to enhance capture efficiency, resulting in significantly amplified electrochemical signals for quantifying target CTCs. Detectable signals occur only when both antibodies are simultaneously present on the cell membrane, greatly enhancing the accuracy of CTCs analysis. The electrochemical biosensor developed in this study exhibited exceptional selectivity in distinguishing target cells from a wide array of cancer cells, achieving a detection threshold as low as 10 cells per milliliter. The biosensor remains stable in the whole blood environment during detection, indicating strong resistance to interference. This dual-signal-amplified electrochemical biosensor shows significant potential for clinical applications in cancer diagnosis and personalized medical treatments.

Received 15th January 2025
Accepted 3rd June 2025

DOI: 10.1039/d5ra00364d

rsc.li/rsc-advances



## 1 Introduction

Breast cancer has become the most prevalent malignant tumor among women globally, causing severe damage to physical and mental health. Early detection and intervention can significantly improve treatment outcomes and survival rates in cancer patients. Compared to traditional tissue biopsy methods, liquid biopsy offers lower invasiveness and convenience,[1,2] Circulating tumor cells (CTCs) are considered ideal targets in the liquid biopsy process for cancer patients.[3] CTCs dissociated from the primary tumors or metastatic foci and enter the circulatory system.[4] These cells can invade neighboring tissues, disseminate through the lymphatic or circulatory systems, and establish new metastatic foci in distant organs, ultimately facilitating cancer progression and metastasis.[5] Rapid, sensitive, and accurate detection of CTCs has crucial clinical implications, enabling early diagnosis, monitoring of disease progression, and evaluation of therapeutic efficacy. Various methodologies for detecting CTCs are currently under rigorous investigation,[6] including surface-enhanced Raman scattering,[7] electrochemiluminescence (ECL) biosensing,[8,9] fluorescence imaging (FI),[10] and inductively coupled plasma mass spectrometry (ICP-MS).[11] These techniques are highly sensitive but often present challenges, including complex instrumentation, the need for specialized equipment and trained personnel, lengthy pre-processing times, and high analytical costs.[12] In contrast, electrochemical biosensors (ECBs) offer several advantages, such as simple equipment, high sensitivity, cost-effectiveness, and ease of automation, which make them promising candidates for CTCs detection.[13,14] Recent advancements in electrochemical sensors have led to significant results in the quantitative detection of CTCs, particularly through nanomaterial-based methods.[15,16] The concentration of CTCs in blood samples is extremely low and exhibits heterogeneity, posing a severe challenge for detection.[17] This approach faces sensitivity limitations due to two main factors: (1) the morphology of the interface restricts the number of signaling probes, reducing effective binding to affinity sites on CTCs,[18] (2) the limited number of non-conducting target CTCs hampers electron transfer between the signaling probe and the electrode, further constraining sensor sensitivity.[19]

[a]*School of Medicine, Jianghan University, Wuhan 430056, China. E-mail: benyali@jhun.edu.cn*

[b]*Department of Dermatology, Huangshi Central Hospital, Affiliated Hospital of Hubei Polytechnic University, Huangshi 435000, China. E-mail: liyu295@hotmail.com*

[c]*School of Electronic and Electrical Engineering, Wuhan Textile University, Wuhan 430200, China*

† Electronic supplementary information (ESI) available. See DOI: https://doi.org/10.1039/d5ra00364d

To address these issues, a novel dual-signal electrochemical biosensor construction method was developed to overcome the sensitivity limitations inherent in traditional configurations.[20,21] This approach involved constructing a GO-SA-EpCAM-CTCs-MWCNTs-COOH-HRP-CA153 sandwich-type biosensor for CTCs recognition.[22] This 3D PVDF/CS nanofibers structure simulates the natural extracellular matrix, providing an ideal microenvironment for cell capture, its high specific surface area and porosity increase antibody binding sites.[23,24] Moreover, PVDF possesses excellent surface properties, non-toxicity, and ion conductivity, while chitosan exhibits good adhesiveness, non-toxicity, and a rich presence of active amino groups. GO and MWCNT-COOH are two-dimensional flexible nanomaterials excellent biocompatibility, vast surface area, remarkable conductivity,and high carrier mobility,[25,26] making them exceptional platforms for electrochemical biosensor production. This innovative design serves two purposes: first, PVDF/CS nanofibers have a large specific surface area and adhesive properties, allowing for GO/SA-$Ab_1$ to be evenly distributed on the nanofibers microchips. Which increases effective binding to affinity sites on CTCs and enhances cell capture efficiency. Second, this design amplifies the electron transfer efficiency between the biosensor and the electrode surface,[27] resulting in enhanced electrochemical performance and detection sensitivity.

In this study, a sandwich structure consisting of GO-SA-EpCAM-CTCs-MWCNTs-COOH-HRP-CA153 was designed on PVDF/CS nanofibrous microchips for the specific capture of MCF-7 cells. When MWCNTs-COOH-HRP-CA153 binds specifically to the circulating tumor cells,[28] HRP catalyzes the decomposition of $H_2O_2$, transforming it into water and oxygen while transferring electrons to $Fe(CN)_6^{3-}$, thus forming $Fe(CN)_6^{4-}$. The generated current signal is linearly related to the number of captured target cells. By employing square wave voltammetry (SWV), this electrochemical signal can be effectively detected and correlated with the quantity of target cancer cells captured. Conversely, if CTCs do not bind with MWCNTs-COOH-HRP-CA153, a series of reaction signals will not be produced, as illustrated in Fig. 1. Additionally, a 3D nanofiber membrane was utilized, incorporating dual nanocomposite materials as signaling elements for the fabrication of the electrochemical biosensor. This mechanism not only enhances detection sensitivity and specificity but also provides a reliable technological pathway for the clinical diagnosis of cancer cells.

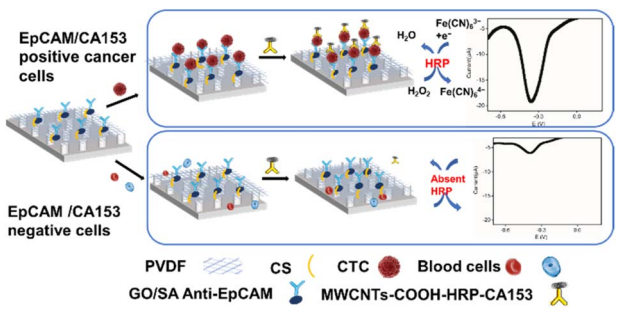


Fig. 1 Schematic of the dual-signal-amplified electrochemical biosensor for cancer cells detection.

## 2 Experimental

### 2.1 Materials and reagents

SU-8 3050 and SU-8 developer were procured from Microchem (Newton,MA, United States). Polydimethylsiloxane (PDMS) prepolymer (Sylgard 184) and its corresponding curing agent were obtained from Dow Corning (Midland, MI, United States). Trichloro(octadecyl)silane and fluorescein diacetate (FDA) were purchased from Sigma-Aldrich (St.Louis, Maryland,United States). Chitosan (CS) was sourced from Ruji Biotech Development Co, Ltd (Shanghai, China). Carbohydrate antigen 153 (CA153) and anti-epithelial adhesion molecule (EpCAM) antibody were purchased from Sangon Biotechnology Co., Ltd (Shanghai, China). Pan-Cytokeratin anti body (C11) Alexa Fluor@488 was purchased from Santa Cruz Biotechnology. CD45 Antibody CoraLite@594 was purchased from Proteintech Group, Inc. DAPI was purchased from Beyotime Biotechnology. The acquisition of the human breast cancer cell line MCF-7 and cervical cancer cell line HeLa were purchased from Shanghai Fuheng Biotechnology Co., Ltd (Shanghai, China). Graphene oxide (GO) dispersion and carboxylated multi-wall carbon nanotubes (MWCNT-COOH) were procured from Nanjing XFNANO Materials Tech Co., Ltd (Nanjing, China). Perylene-3,4,9,10-hydroxysuccinimide (NHS) and 1-ethyl-3-(3-dimethylaminopropyl)-carbodiimide (EDC) were obtained from Macklin Technology Co., Ltd, (Shanghai, China). Cancer patient serum samples were provided by Huangshi Central Hospital (Huangshi, China). Human embryonic kidney cell line (293T),human colon cancer cells (HT-29) were purchased from the American Type Culture Collection (ATCC). Throughout the experimental process, Deionized water generated from Millipore was used.

### 2.2 Cell culture

Human breast carcinoma cells (MCF-7),human embryonic kidney cell line (293T),human colon cancer cells (HT-29),and human cervical cancer cells (HeLa) were cultivated in Dulbecco's Modified Eagle Medium (DMEM). All the aforementioned cell lines were consistently maintained in a cell incubator (37 °C, 5% $CO_2$),the cells underwent digestion with a solution containing 0.25% trypsin and 0.02% EDTA for a duration of 1 to 2 minutes. The detached cells were then collected and transferred to fresh growth medium for replating.

### 2.3 Fabrication of the PDMS micropillars and PVDF/CS nanofibers electrospinning

For the nanofiber electrospinning, 200 mg PVDF and 10 mg CS powder were dissolved in 1 mL solvent (*N*, *N*-dimethylformamide and acetone, 6 : 4) under magnetic stirring for 6 hours to obtain a homogeneous solution. As shown in Fig. 2a, horizontally mounted grounded PDMS micropillars were used as the PVDF/CS nanofibers collectors. The density of nanofibers can be controlled by the electrospinning voltage, the velocity of PVDF/

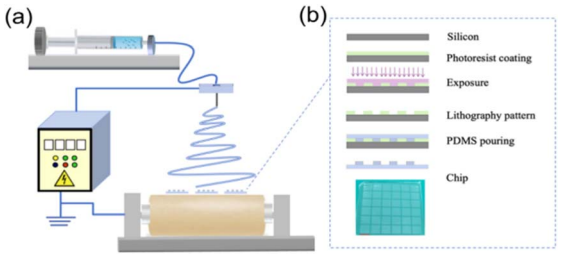


Fig. 2 Process of fabrication of (a) the electrospinning PVDF/CS nanofibers and (b) PDMS micropillar substrate using soft photolithography.

CS solution and the electrospinning time.[29] The progress of PDMS micropillars fabrication is illustrated in Fig. 2b. The microstructures on the SU-8 molds, consisting of cylindrical columns, which were fabricated through standard soft photolithography. Firstly, SU-8 3050 photoresist was deposited onto a Silicon wafer with a spin-coating process, 3000 rpm for 40 seconds. Subsequently,a soft baking procedure was performed, initially at a temperature of 65 °C for 5 minutes, followed by an elevation to 95 °C for an additional 30 minutes. After exposed, a rigorous baking process was conducted at a temperature of 65 °C for a 1 minute and 95 °C for 5 minutes. Upon completion of the baking stages, the molds underwent development in SU-8 developer solution.[30] Subsequently, they were meticulously cleaned with isopropyl alcohol and thoroughly dried. In order to prepare the PDMS gel, PDMS prepolymer and curing agent with a weight ratio of 10 : 1 was mixed and then degassed for 15 minutes. A small amount of PDMS gel was carefully dispensed through a needle into the mold's reservoir, allowing capillary action to fill the microstructure trenches. The PDMS gel underwent a curing process within a vacuum oven, maintained at a temperature of 60 °C for two hours. The height of the PDMS micropillars was 40 μm, and the diameter and spacing of the columns were 50 μm.

### 2.4 Preparation of GO-SA-$Ab_1$/MWCNT-COOH-HRP-$Ab_2$ DNA probes

100 mg graphene oxide (GO) was added into 200 mL chitosan solution (0.05% (w/v) in anhydrous ethanol) under ultrasonic for 30 minutes. Subsequently, 1 mL GO solution was mixed with 1 mL MES solution (0.1 mol $L^{-1}$) and agitated at ambient temperature for a duration of 2 hours to activate the carboxyl functionalities present on the surface of the GO. The resulting pellet underwent a rigorous washing procedure, involving five consecutive rinses with Phosphate Buffered Saline (PBS) buffer. Next, 1 mL streptavidin (SA) solution (50 μg $mL^{-1}$) was added to the pellet. The pellet underwent a rigorous washing process five times with PBS buffer to effectively eliminate any unbound SA. Following this thorough washing, the cleaned pellet was resuspended in precisely 1 mL PBS buffer. Following the process, the micropillar surface underwent a meticulous washing procedure, involving gentle rinsing with PBS buffer three separate times. Subsequently, 200 μL precisely diluted *anti*-EpCAM (Ab1) antibody solution (ratio of 1 : 5000) was carefully dispensed onto the dried micropillar surface and incubated for 2 hours at ambient temperature. Afterward, the nanofiber-micropillar was washed and dried, completing the modification of GO/SA-Ab1 to obtain the functionalized film.

For the preparation of the HRP-MWCNTs-COOH-$Ab_2$ complex, EDC and NHS were dissolved in 0.1 mol $L^{-1}$ MES solution (pH 5.2) with a concentration of 0.4 mmol $L^{-1}$ and 0.1 mmol $L^{-1}$, respectively. Then, 2 mg MWCNTs-COOH was added into 4 mL of the prepared EDC/NHS solution under ultrasonic for 1 minute. After centrifuged at a speed of 5000 rpm for 10 minutes, the pellet should be thoroughly washed with Phosphate Buffered Saline (PBS) buffer five times to effectively remove any excess EDC and NHS. Following washing, 0.5 mL breast cancer-related antibody (Anti-CA153, $Ab_2$) (400 ng $mL^{-1}$) and 0.5 mL HRP (80 μg $mL^{-1}$) were added into the mixture, thoroughly sonicated the mixture in an ice bath for 5 minutes. Then, the mixture should be agitated for a period of one night to ensure proper blending. 0.05% Tween 20 solution was mixed with 1% BSA with a ratio of 1 : 10 and stirred overnight at room temperature. It is essential to centrifuge the antibody complex mixture at a speed of 5000 rpm for 10 minutes. Following this step, the resulting pellet should be thoroughly washed with PBS buffer to remove any excess horseradish peroxidase (HRP) and antibody 2 ($Ab_2$). Next, the Tween 20 and BSA mixture was added into the antibody complex pellet at room temperature and maintained for 90 minutes. Following the completion of the reaction, the mixture was centrifuged at a speed of 5000 rpm for 10 minutes. Subsequently, wash the pellet with Phosphate Buffered Saline (PBS) buffer five times to effectively remove any excess antibodies and BSA. The HRP-MWCNTs-COOH-$Ab_2$ complex in PBS buffer containing 3% BSA was stored at 4 °C for future use.

### 2.5 Cancer cell capture and SEM characterization

The microchips, specifically designed for capturing cancer cells, underwent three rigorous washes, followed by the incubation of primary antibodies. Subsequently, $1 \times 10^6$ cells were meticulously added onto each chip. These microchips were incubated for 40 minutes in a cell incubator (37 °C, 5% $CO_2$) to ensure optimal conditions for cell incubation. For scanning electron microscopy (SEM) characterization, the chips containing the captured cells were initially fixed by 2.5% glutaraldehyde for 2 hours. Subsequently, the chips underwent immersion in a sequential series of ethanol solutions, with concentration of 30%, 50%, 70%, 80%, 90%, 95% and 100%, respectively, followed by overnight air drying. The Scanning Electron Microscopy (SEM) analysis was performed under a rigorously controlled accelerating voltage of 10 kV. Before the commencement of the measurements, the specimens were thoroughly and precisely coated with a layer of gold film, utilizing the sputter coating methodology.

### 2.6 Preparation and detection of electrochemical sensors

Firstly, 200 μL GO/SA suspension was uniformly spread onto the surface of microchips, followed by incubation at room temperature for 1 hour. After gently washed three times with PBS, 200 μL 1 : 5000 diluted *anti*-EpCAM solution ($Ab_1$) was added dropwise to the microchips surface and incubated for 2

hours at room temperature. After washing with PBS for three times, the functionalized film was obtained, where the GO/SA-$Ab_1$ was successfully modified. The GO/SA-$Ab_1$-modified microchips were then incubated with 100 μL cell suspension or blood samples for 50 minutes at 37 °C in a 5% $CO_2$ incubator. Then, the microchips were gently rinsed three times with PBS to remove the non-specifically adsorbed cells. To complete the construction of the super sandwich structure, 200 μL carboxylated multi-walled carbon nanotube-horseradish peroxidase-carbohydrate antigen153 (MWCNTs-COOH-HRP-$Ab_2$) complex was added and incubated for 50 minutes in a cell culture incubator. Due to the excellent electrical conductivity of MWCNTs-COOH and the catalytic activity of HRP in the redox reaction involving hydrogen peroxide ($H_2O_2$), a significant amplification of the signal at the antigen–antibody binding sites was achieved, as shown in Fig. 1. The microchips were then analyzed using an electrochemical workstation (CHI 660, CH Instruments Inc., Shanghai, China). For each experimental group, two microchips were prepared as controls to ensure the reproducibility of the results. A three-electrode system was employed for electrochemical detection, utilizing an Ag/AgCl reference electrode, a platinum wire auxiliary electrode, and the microchips as the working electrode. Square wave voltammetry (SWV) and tests were conducted. To validate the sequential modification steps of the electrode, SWV characterizations were performed in a $Fe(CN)6]^{3-/4-}$ solution (1 mM) containing 0.1 M KCL. The electrochemical experiments were performed in the electrochemical cell containing PBS (0.1 M, pH 7) with $H_2O_2$. The electrochemical response was quantitatively assessed through SWV measurements within a potential range of 0 V to −0.6 V, while the step potential and frequency were 15 mV and 50 Hz, respectively.

### 2.7 Electrochemical detection of MCF-7 cells

The GO/SA-$Ab_1$-modified microchips were incubated in various concentrations of MCF-7 cell in DMEM solution for 40 minutes at 37 °C. Then, the biosensors were incubated with 200 μL carboxylated multi-walled carbon nanotube-horseradish peroxidase-carbohydrate antigen 153 (MWCNTs-COOH-HRP-CA153) antibody complex for 50 minutes at 37 °C. Finally, the microchips were gently washed three times with PBS, and analyzed using an electrochemical workstation. To assess the electrochemical platform effectiveness for analyzing biological samples, specific number of MCF-7 cells were spiked into the collected whole blood samples and analyzed by the constructed biosensor.

### 2.8 Pretreatment of clinical samples

With approval from the Huangshi Central Hospital, human peripheral blood samples from 12 individuals were collected in their entirety, including 3 healthy donors, 3 cervical cancer patients, and 6 breast cancer patients. The study was conducted in accordance with the guidelines of the Declaration of Helsinki. The experiments involving human blood samples were approved by the Ethics Committee of [Institution Name: School of Medicine, Jianghan University], with approval number [YXLL2021-006]. Written informed consent was obtained from all donors prior to sample collection. Throughout the experimental process, no further processing was performed on the blood samples. The cell suspension was replaced with a direct drop of 100 μL anticoagulated blood, and other experimental steps remained unchanged. The recovery and capture efficiency were defined as the ratio of the number of captured cells to the number ofinitially introduced cells.

## 3 Result and discussion

### 3.1 Preparation and characterization of PVDF/CS nanofibers

The PVDF/CS solution was processed using a high-voltage electrostatic spinning technique, resulting in a mesh structure on a PDMS micropillar chips, as shown in Fig. 3a. Form the SEM characterization in Fig. 3b, PVDF/CS nanofibers displayed a smooth morphology and a uniform diameter distribution (average diameter was 487 ± 50 nm) and a randomly oriented porous structure. The density of nanofibers can be controlled by the electrospinning time. As shown in Fig. 3c, when the electrospinning time was increased from 0 minute to 10 minutes, the nanofibers numbers increased. MCF-7 cells were selected as the model target cells to determine the optimal spinning duration for cell capture experiments. The results in Fig. 3d shown that the cell capture efficiency on the 10 minutes electrospinning substrate was about 4 times than that on nanofibers-free substrate. When the electrospinning time was more than 6 minutes, the cell capture efficiency was almost saturation, therefore, the 6 minutes electrospinning substrates were used in the following cell experiments.

### 3.2 Efficient capture of CTCs with different structured chips

To further assess the advantages of bio-interface for capturing cancer cells, three different substrates, flat PDMS, PDMS micropillars and PDMS micropillars coupled with PVDF/CS nanofibers, were used to capture MCF-7 cancer cells. As shown in Fig. 4, the results indicated that there were almost no

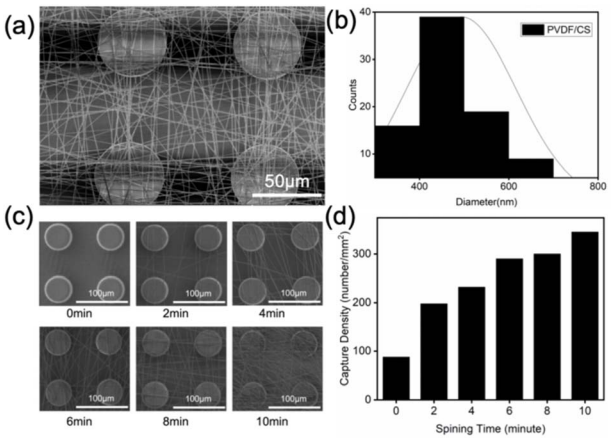


Fig. 3 SEM image of 3D PVDF/CS micro-nano chip. (b) The diameter distribution of PVDF/CS nanofibers after electrospinning. (c) SEM images of the micro-nano chips with different electrospinning time. (d) Cancer cells Capture density on micro-nano chips with different spinning times. Scale bars in (a) and (c) are 50 μm.

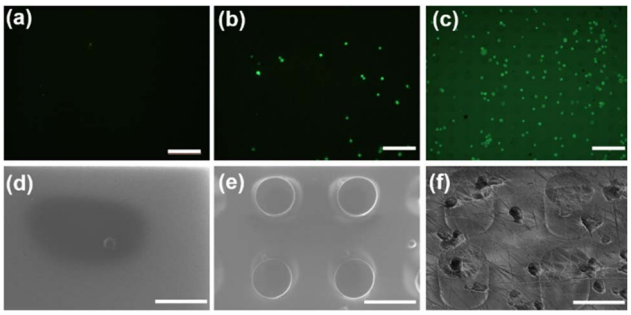


Fig. 4 Fluorescence images of cancer cells captured on different topographic substrates: (a) flat PDMS substrate, (b) PDMS micropillars substrate and (c) PDMS micropillars coupled with PVDF/CS nanofiber substrate. (c–e) SEM images of cancer cells captured on the different topological substrates. Scale bars are 200 μm in (a–c) and 50 μm in (d–f), respectively.

cells captured on the flat substrate. Compared to the flat substrate in Fig. 4a, the micropillars structure in Fig. 4b exhibited a significantly higher capture efficiency. When the PVDF/CS nanofibers were coupled with PDMS micropillars, as shown in Fig. 4c, the cancer cells capture efficiency was approximately four times than that on PDMS micropillars substrate in Fig. 4b. This enhancement suggests that the spun microcolumn structure, combined with GO/SA-$Ab_1$ modification, greatly improves capture efficiency. Moreover, specific capture of EpCAM-overexpressing tumor cells was achieved by functionalizing the nanofiber micropillar surface with GO-SA-$Ab_1$. These results can also be found from the SEM characterization, as shown in Fig. 4d–f. Under the same conditions, the PVDF/CS nanofibrous microcolumn chip substrate captured the highest number of circulating tumor cells compared to other substrates. The 3D architecture of the spun micropillars contributed to this effect by providing additional binding sites for GO/SA and *anti*-EpCAM. Additionally, this 3D nanofiber mesh also effectively mimicking the extracellular matrix, thereby enhancing topological interactions between cancer cells and the nanofibers.

### 3.3 Selectivity, stability, and reproducibility of the biosensor

To evaluate the recognition performance of PVDF/CS nanofibers, MCF-7 cells were employed as positive model cells, while 293T and HeLa were used as negative models. Additionally, DMEM solution was included as a control test. The capture performance across different cancer cell types is illustrated in Fig. 5a. In the presence of non-target cells, the peak currents were observed to closely align with those recorded in the blank control, demonstrating a high selectivity of cells capture. In contrast, a significant increase in SWV values was noted upon the introduction of $10 \times 10^5$ MCF-7 cells, which confirmed the biosensor's specificity for proteins expressed by tumor cells.

### 3.4 Optimization of experimental conditions

To optimize the electrochemical performance of the biosensor, we systematically adjusted the HRP to $Ab_2$ ratio, binding time with MCF-7 cells, and incubation duration. As shown in Fig. 5b

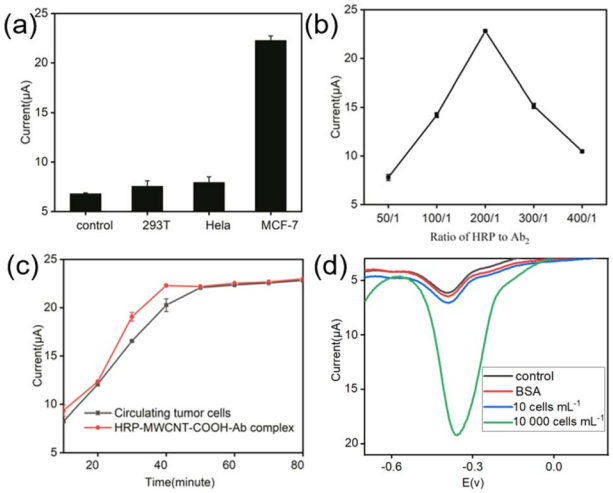


Fig. 5 Current response of biosensor. (a) Current response of chip to different kinds of cells. (b) Effect of the coupling ratio of HRP to $Ab_2$ on the electrochemical performance of the biosensor. (c) Effect of incubation time of cancer cells and HRP-MWCNT-COOH-$Ab_2$ complex on the electrochemical performance of the biosensor. (d) Current response of the chip under different condition.

and S1,† when the ratio of HRP and $Ab_2$ was 200 : 1, the current signal was largest. It was noted that the current signal was increased when the cancer cells incubation time increased, as shown in Fig. 5c and S2.† When the incubation time was larger than 40 minutes, the current signal was no longer increased. Therefore, incubation time of 40 minutes was selected as optimal condition. Similarly, the optimal binding time of the MWCNTs-COOH-HRP-$Ab_2$ complex probe to cancer cells was approximately 50 minutes, as shown in Fig. 5c and S3.† Current response of chip to different conditions was also investigated. Results in Fig. 5d shown that when the cancer cells were added onto the chip, the electrochemical electric signal had a larger response.

### 3.5 Current response of the biosensor

The current response of biosensor was investigated by incubating a series of cell suspensions with varying concentrations of MCF-7 cells and measuring the response currents. Fig. 6a shown the current response curves for different cell concentrations. The SWV peaks observed in the figures are primarily stemming from the reaction between horseradish peroxidase (HRP) catalyzing the transformation of $Fe(CN)_6^{3-}$ to $Fe(CN)_6^{4-}$

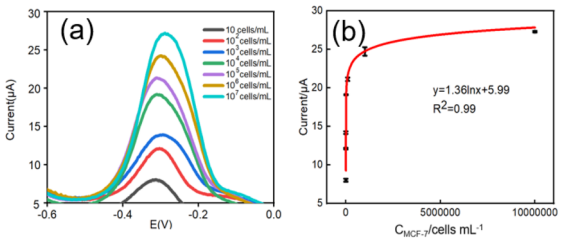


Fig. 6 (a) Current response of the biosensor to the different concentration of MCF-7 cancer cells. (b) The relationship of the current response and cancer cells concentration.

in the presence of hydrogen peroxide ($H_2O_2$). HRP acts on $H_2O_2$, facilitating its conversion and leading to the generation of detectable current signals. These current signals reflect the amount of target cancer cells captured, demonstrating the sensitivity and specificity of the biosensor approach. As the cell concentration ($10^1$–$10^7$ cells per mL) increases from 10 to $10^7$ $mL^{-1}$, the oxidation current response of the immunosensor also increases gradually. A standard curve relating peak current to cell concentration was established in Fig. 6b. The analysis reveals a strong linear correlation between the logarithm of peak current and cell concentration ($10^1$–$10^7$ $mL^{-1}$). According to the fitted linear regression equation in Fig. 6b, the immunosensor's lowest detection limit is determined to be 10 cells per mL, with a detection range spanning from $10^1$ to $10^7$ cells per mL. This detection limit indicated that the dual signal amplification effect of GO and MWCNTs-COOH, along with the super sandwich structure primarily composed of $Ab_1$-CTCs-$Ab_2$, significantly enhances the sensitivity of the immunosensor. This advancement provides promising potential for detecting blood samples from clinical patients.

### 3.6 Evaluation of blood samples by biosensors

To assess the feasibility of the biosensor developed in this study for monitoring blood samples and its potential for clinical application, we randomly selected five blood samples from healthy individuals. Following a standardized operating procedure, MCF-7 cells were added to these samples to achieve final concentrations of $10^1$, $10^2$, $10^3$, $10^4$, and $10^5$ cells per mL. Subsequently, 200 μL of the mixed solution was added onto the surface of the pre-modified GO/SA Anti-EpCAM microchip and incubated for 40 minutes, consistent with prior immunosensor construction steps. The samples were then analyzed using an electrochemical workstation, where the peak current values obtained were substituted into a previously established regression equation correlating cell concentration with peak current. This facilitated the calculation of the biosensor's detection recovery rate, providing insight into its effectiveness for clinical blood sample analysis. As presented in Table 1, the immunosensor demonstrated a detection recovery rate exceeding 85% in blood samples containing standardized tumor cells. These results indicate that the biosensor is feasible for detecting CTCs in clinical blood samples. The developed electrochemical biosensor demonstrates enhanced sensitivity, efficiency, and simplicity, making it crucial for accurately distinguishing MCF-7 cells from blood cells in clinical applications.

Table 1 Biosensor detects MCF-7 cells in blood samples[a]

| Sample no. | Know (cell $mL^{-1}$) | Cytosensor (cell $mL^{-1}$) | Recovery (%) | RSD ($n = 3$) |
|---|---|---|---|---|
| 1 | $1 \times 10^5$ | $0.97 \times 10^5$ | 96.79 | 0.56 |
| 2 | $1 \times 10^4$ | $0.99 \times 10^4$ | 99.17 | 0.65 |
| 3 | $1 \times 10^3$ | $1.09 \times 10^3$ | 109.23 | 0.66 |
| 4 | $1 \times 10^2$ | $0.98 \times 10^2$ | 98.25 | 0.67 |
| 5 | $1 \times 10^1$ | $0.85 \times 10^1$ | 85.24 | 0.67 |

[a] RSD: relative standard deviation.

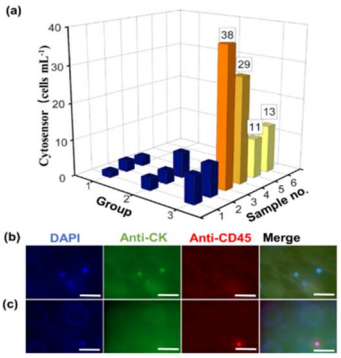


Fig. 7 (a) CTCs captured from the human peripheral blood samples. Immunofluorescence stain of (b) cancer cells and (c) white blood cell: DAPI (blue) for nucleus, Pan-Cytokeratin anti body (C11) Alexa Fluor® 488 (green) for CK and Alexa Fluor® 594 (red) for CD45. Cells with DAPI+/CK+/CD45-are identified as CTCs, while leukocytes were identified as CK-/DAPI+/CD45+.

### 3.7 Clinical utility assessment

Whole blood samples were collected from three healthy donors (group 1 in Fig. 7a) and nine cancer patient donors, including 3 cervical cancer patients (group 2 in Fig. 7a) and 6 breast cancer patients (group 3 in Fig. 7a). The constructed electrochemical biosensor successfully detected rare CTCs in human serum, achieving a 66% capture efficiency and demonstrating good stability in complex biological matrices. Validation of the biosensor using patient blood samples revealed that the collected CTCs were CD45- (red)/4′,6-diamidino-2-phenylindole (DAPI)+ (blue)/CK+ (green) cells (Fig. 7b), while leukocytes were identified as CK-/DAPI+/CD45+ (Fig. 7c), confirming efficient sorting of CTCs.

## 4 Conclusions

In conclusion, we have successfully developed a novel approach for cancer cell analysis. The PVDF/CS membrane serves a critical role as a carrier in the capture and enrichment of CTCs. Its excellent specific surface area and biocompatibility contribute significantly binding efficiency. The high sensitive and specific of biosensing platform can be largely attributed to GO-SA-EpCAM-CTCs-MWCNTs-COOH-HRP-CA153 sandwich-type biosensor, as well as the exceptional electronic conductivity provided by the integration of GO and MWCNTs-COOH into the sensing interface. The introduction of HRP enables the generation of measurable electrochemical signals through its catalyzed redox reactions. The core mechanism for signal generation is the redox reaction between $Fe(CN)_6^{3-/4-}$ and $H_2O_2$ catalyzed by HRP. The electrochemical signal produced from this reaction is proportional to the binding amount of target cells, effectively reflecting the presence of CTCs. The biosensor exhibits a linear response for MCF-7 cell concentrations ranging from 10 to $1 \times 10^7$ cells per mL, with a limit of detection (LOD) of less than 10 cells per mL. Research indecates that approximately 40–60% of breast cancer patients have significantly elevated CA15-3 levels.[31] In this experiment, the biosensor constructed with CA15-3 antibodies achieved a detection rate of 66% in breast cancer patients, while maintaining excellent

stability. This impressive performance is due to the biosensor's dual recognition design, which enhances specificity and accuracy in target cells detection. We believe the developed electrochemical biosensors possess significant potential for clinical applications in CTCs detection. Facilitating early cancer screening and enabling the evaluation of anti-cancer therapies, ultimately contributing to improved patient outcomes. Future studies will focus on optimizing the biosensor for a broader range of cancer types and exploring its integration into point-of-care diagnostic tools.

## Data availability

The authors confirm that the data supporting the findings of this study are available within the article.

## Author contributions

Yujuan Wu: constructed the cytosensor, engaged in data curation, and participated in writing, reviewing, and editing of the manuscript. Yi Wang also conducted data curation, review, and editing. Rongxiang He: contributed to the fabrication of chips and the development of the instrument system. Yu Li: conducted sample collection and analysis. Yali Ben: Assumed project administration, conceptualization, methodology development, supervision, resource allocation, and funding acquisition. All authors read and approved the final manuscript.

## Conflicts of interest

There are no conflicts to declare.

## Acknowledgements

Financial support from the National Natural Science Foundation of China (11804121) are gratefully acknowledged. Special Funds for Central Guiding Local Scientific and Technological Development Project (2016ZYYD049) are gratefully acknowledged.

## References

1 M. Kalimutho, K. Nones, S. Srihari, P. H. G. Duijf, N. Waddell and K. K. Khanna, *Trends Pharmacol. Sci.*, 2019, **40**, 198–211.
2 X. Wen, X. Guo, S. H. Wang, Z. H. Lu and Y. D. Zhang, *Biocybern. Biomed. Eng.*, 2024, **44**, 119–148.
3 D. J. Smit and K. Pantel, *Mol. Aspects Med.*, 2024, **96**, 101258–101264.
4 J. Zhang, H. Zhou, T. Hao, Y. Yang, Q. Zhang, J. Li, M. Ye, Y. Wu, W. Gao and Z. Guo, *Anal. Chim. Acta*, 2023, **1271**, 341465–341472.
5 X. Wang, L. Wang, H. Lin, Y. Zhu, D. Huang, M. Lai, X. Xi, J. Huang, W. Zhang and T. Zhong, *Front. Oncol.*, 2024, **14**, 1303335–1303356.
6 H. Safarpour, S. Dehghani, R. Nosrati, N. Zebardast, M. Alibolandi, A. Mokhtarzadeh and M. Ramezani, *Biosens. Bioelectron.*, 2020, **148**, 111833–111851.
7 J. Wang, K. M. Koo and M. Trau, *Anal. Chem.*, 2022, **94**, 14906–14916.
8 E. Yang, Y. Zhang and Y. Shen, *Anal. Chim. Acta*, 2022, **1209**, 339140–339160.
9 P. Liu, L. Wang, K. Zhao, Z. Liu, H. Cao, S. Ye and G. Liang, *Sens. Actuators, B*, 2020, **316**, 128131–128137.
10 P. Chen, Y. He, T. Liu, F. Li, K. Huang, D. Tang, P. Jiang, S. Wang, J. Zhou, J. Huang, Y. Xie, Y. Wei, J. Chen, W. Hu and B. Ying, *Biosens. Bioelectron.*, 2022, **202**, 114009–114018.
11 X. Yin, B. Chen, M. He and B. Hu, *Anal. Chem.*, 2020, **92**, 10308–10315.
12 S. He, J. Wei, L. Ding, X. Yang and Y. Wu, *Talanta*, 2022, **239**, 123024–123038.
13 X. Su, Q. You, L. Zhuang, Z. Chang, M. Ge, L. Yang and W.-F. Dong, *J. Pharmaceut. Biomed.*, 2023, **234**, 115479–115487.
14 X. Zhang, X. Jiang, W. Wang, S. Luo, S. Guan, W. Li, B. Situ, B. Li, Y. Zhang and L. Zheng, *Microchim. Acta*, 2023, **190**, 65–73.
15 N. Yu, G. Ma, Y. Chen, S. Huang, Y. Gong, S. Li, H. Gu, H. You and P. Miao, *Colloids Surf., B*, 2023, **229**, 113482–113488.
16 M. Dong, Z. Gao, Y. Zhang, J. Cai, J. Li, P. Xu, H. Jiang, J. Gu and J. Wang, *RSC Adv.*, 2023, **13**, 12966–12972.
17 D. Sun, J. Lu, L. Zhang and Z. Chen, *Anal. Chim. Acta*, 2019, **1082**, 1–17.
18 S. Samanman, A. Numnuam, W. Limbut, P. Kanatharana and P. Thavarungkul, *Anal. Chim. Acta*, 2015, **853**, 521–532.
19 Z. Li, G. Wang, Y. Shen, N. Guo and N. Ma, *Adv. Funct. Mater.*, 2018, **28**, 1707152–1707162.
20 Y. Peng, B. Lu, Y. Deng, N. Yang and G. Li, *Biosens. Bioelectron.*, 2022, **201**, 113973–113979.
21 A. Bagheri Hashkavayi, B. S. Cha, S. H. Hwang, J. Kim and K. S. Park, *Sens. Actuators, B*, 2021, **343**, 130087–130092.
22 Y. Nie, P. Wang, Q. Ma and X. Su, *Anal. Chem.*, 2022, **94**, 11016–11022.
23 S. A. Salim, S. A. Loutfy, E. M. El-Fakharany, T. H. Taha, Y. Hussien and E. A. Kamoun, *J. Drug Deliv. Sci. Tec.*, 2021, **62**, 102417–102426.
24 J. Frigaard, J. L. Jensen, H. K. Galtung and M. Hiorth, *Front. Pharmacol.*, 2022, **13**, 880377–880395.
25 M. Al Kausor, S. S. Gupta and D. Chakrabortty, *Chem. Pap.*, 2024, **78**, 6259–6285.
26 S. Feng, M. Yan, Y. Xue, J. Huang and X. Yang, *Chem. Commun.*, 2022, **58**, 6092–6095.
27 X. Wu, T. Xiao, Z. Luo, R. He, Y. Cao, Z. Guo, W. Zhang and Y. Chen, *J. Nanobiotechnol.*, 2018, **16**, 65–73.
28 L. Jia, G. H. Li, N. Ma, A. M. Zhang, Y. L. Zhou, L. Ren and D. Dong, *Bmc Cancer*, 2022, **22**, 760–769.
29 K. Zhou, X. G. Zhu, Y. Li and J. Liu, *RSC Adv.*, 2014, **4**, 31988–31993.
30 M. Qi, M. Ruan, J. Liang, Z. Zhang, C. Chen, Y. Cao and R. He, *Materials*, 2023, **16**, 3065–3075.
31 K. S. Hu, Y. C. Wang, Y. Ma and C. Xiu, *Oncol. Lett.*, 2025, **29**, 133–140.